

# THE GAURIBIDANUR RADIOHELIOGRAPH

R. RAMESH, K. R. SUBRAMANIAN, M. S. SUNDARARAJAN and CH. V. SASTRY  
*Indian Institute of Astrophysics, Bangalore 560034, India*

(Received 16 December 1997; accepted 16 February 1998)

**Abstract.** A new radio heliograph for obtaining two-dimensional images of the solar corona sequentially at many frequencies in the range 40–150 MHz has been built by the Indian Institute of Astrophysics at the Gauribidanur Radio Observatory (lat.  $13^{\circ}36'12''$  N and long.  $77^{\circ}27'07''$  E) about 100 km north of Bangalore, India. This paper describes various aspects of the antenna system, receiver front end, digital hardware, the data acquisition and the calibration procedure. The performance of the instrument is illustrated with maps of the continuum emission from the undisturbed corona at different frequencies.

## 1. Introduction

Ever since the de-commissioning of the Clark Lake radio heliograph (Erickson, Mahoney, and Erb, 1982) in 1984, there has been no other radio telescope fully dedicated to observing the solar corona at frequencies  $\leq 150$  MHz. In the present day scenario where several instruments operating at various frequency bands are fully dedicated for solar observations both from ground and space, collaborative studies using data obtained at different frequencies are proving to be very helpful in understanding various phenomena that take place in the solar atmosphere. In this connection the newly constructed Gauribidanur radio heliograph (GRH) which can produce two-dimensional pictures of the outer solar corona in the frequency range 40–150 MHz is expected to play an important role, since no other instruments are in operation at present in the above frequency range.

## 2. Array Configuration

The heliograph is a T-shaped array with the long arm (1280 m) in the east-west direction and the short one (441 m) along the south direction. Figure 1 shows the basic element used in the array. It is a Log Periodic Dipole (LPD) with an effective collecting area of  $0.5 \lambda^2$  and a characteristic impedance ( $Z_0$ ) of  $50 \Omega$ . The dipoles are made of aluminium tubes and have been designed to operate in the frequency range 40–150 MHz with a VSWR  $< 2$  and a directional gain of 8 dB. The measured half-power beamwidths are approximately  $60^{\circ}$  in the E-plane and  $100^{\circ}$  in the H-plane, enabling observations to be carried out over a large range of hour angle and declination respectively.



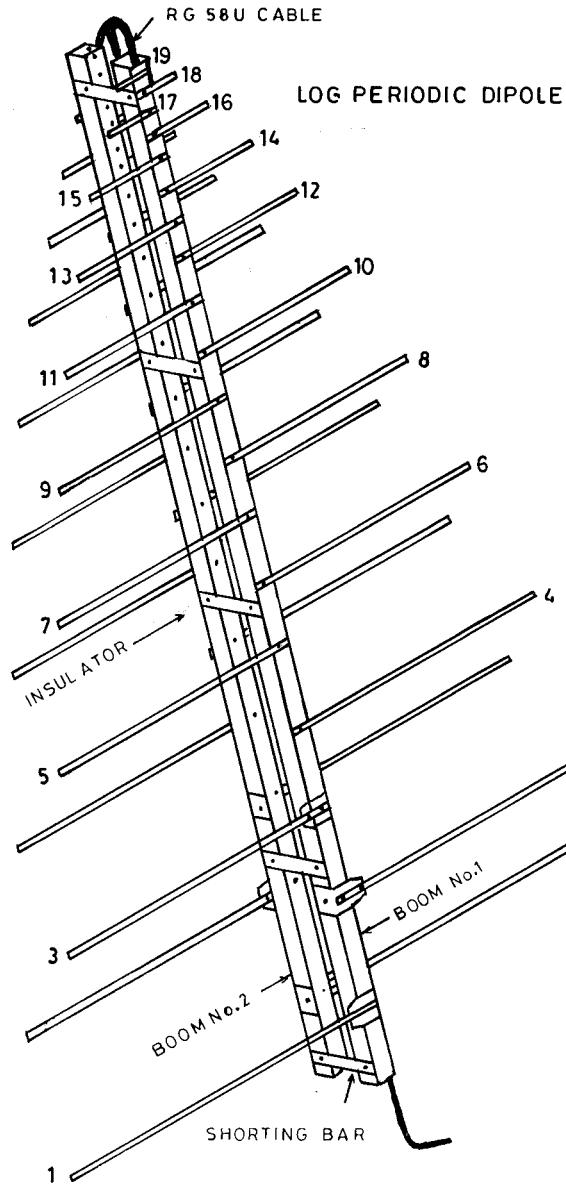


Figure 1. Log periodic dipole used in the Gauribidanur radioheliograph.

The E–W arm has 128 elements separated by 10 m intervals except for the elements 64 and 65, which are separated by 20 m. This is because of the first of the 64 elements in the south arm being located at the center of the E–W arm. The elements are spaced 7 m apart in the south arm. This spacing between the individual elements in the E–W and the south arms gives rise to grating lobes along either direction, which will be discussed in a later section. All the elements

TABLE I  
GRH – specifications and performance

| Parameter                  | Value  |
|----------------------------|--|
| Frequency of operation     | 40–150 MHz   |
| Bandwidth                  | 1 MHz  |
| Basic element              | Log periodic dipole  |
| Effective collecting area  | $96 \lambda^2$   |
| Declination coverage       | $-31^\circ$ S to $+59^\circ$ N   |
| Observing period           | $\pm 2$ hours around local meridian                                    |
| Number of antenna groups   | 32 (16 E–W and 16 south)   |
| Correlation receiver       | 1024 channels (1 bit–2 level)  |
| Sampling rate              | 4 MHz  |
| Sensitivity ( $5 \sigma$ ) | $\approx 2 \times 10^{-2}$ s.f.u. at 150 MHz for 10 s integration time |
| Field of view              | $3^\circ \times 4^\circ$ at 150 MHz                                    |
| Angular resolution         | $5' \times 8'$ (R.A. $\times$ Dec.) at 150 MHz                         |
| Dynamic range of images    | $\approx 20$ dB  |

in the array are oriented in the E–W direction and they accept linear polarisation in that direction. Figures 2 and 3 show a portion of the E–W and south arms of the heliograph. The specifications of the heliograph are given in Table I. The field of view and the angular resolution are frequency dependent. Both of them scale inversely with frequency.

### 3. Element Grouping

The E–W arm is divided into 16 groups of 8 antennas each. The RF signal from each element in a group is passed through a high-pass filter which has a cut-off of 50 MHz and then amplified approximately 30 dB in a wide-band amplifier. This pre-amplifier has a noise figure of  $\approx 3$  dB (300 K) and a bandpass extending from 0.5 to 500 MHz. The high-pass filter is used to cut off large interfering signals at frequencies  $< 40$  MHz, which can give rise to spurious intermodulation products. In addition it also reduces the dynamic range requirements on the subsequent stages of electronics. The signals from the eight elements in a group are then combined in a branched feeder system using power combiners and RG8U cables as shown in Figure 4. All the groups are equally spaced with the spacing between the phase centers of the adjacent groups being 80 m except for the groups  $G_8$  and  $G_9$  whose phase centers are separated by 90 m. This is due to the 20 m spacing between the elements 64 and 65 in the E–W arm as mentioned in the previous section.



*Figure 2.* E-W arm of the GRH.



*Figure 3.* South arm of the GRH.

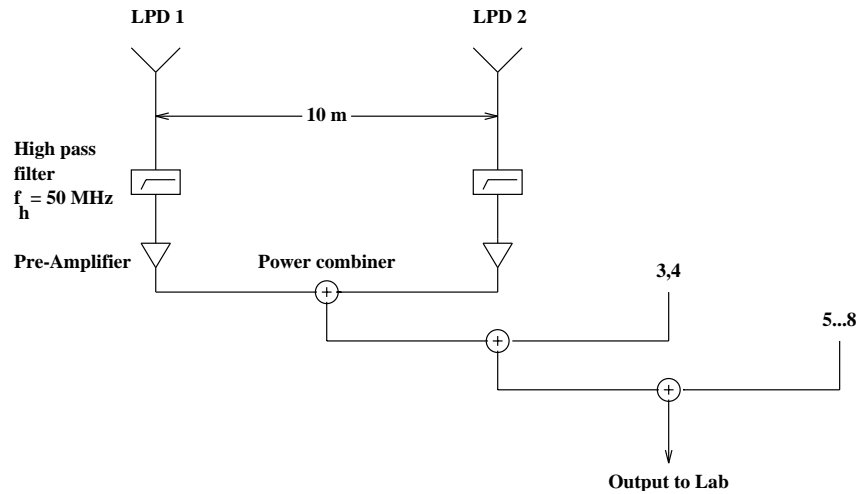


Figure 4. One of the 16 groups in the east-west arm.

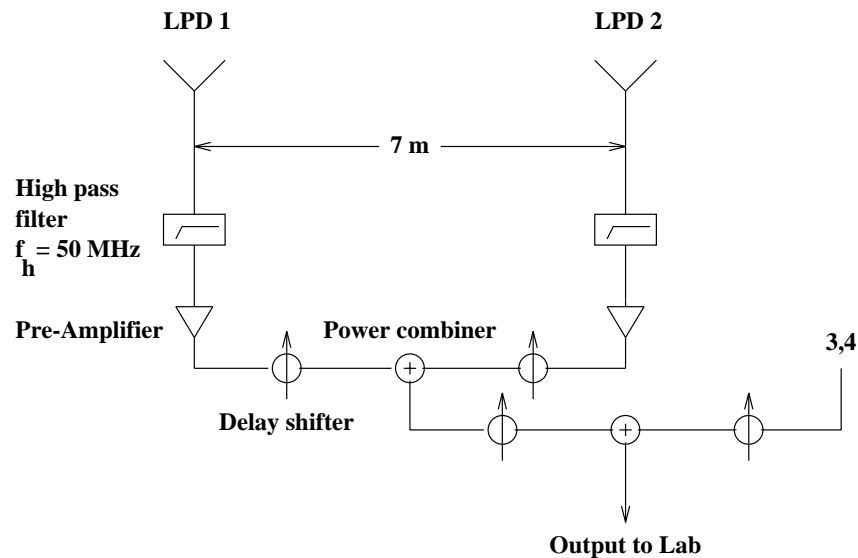


Figure 5. One of the 16 groups in the south arm.

The south arm is also divided into 16 groups but with only 4 elements in each group. Filtered and amplified outputs from the four elements of each group are combined using delay shifters, power combiners and cables as shown in Figure 5. The phase centers of the adjacent groups are equally spaced with an interval of 28 m. Delay shifters are used for changing the direction of the beam of each group to minimise coherence loss when receiving signals from larger zenith distances. A computer-controlled system provides the switching signals for the insertion of the

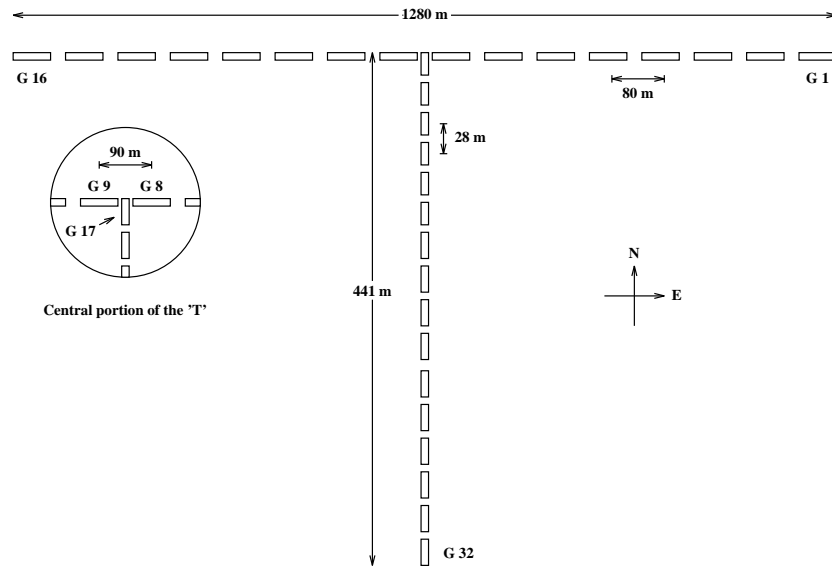


Figure 6. Layout of the Gauribidanur radio heliograph.

required delay in the signal path. Figure 6 shows the arrangement of various groups in the E–W and the south arms of the heliograph.

As the spacing between the individual elements in each group is greater than one wavelength in our frequency range (40–150 MHz) of observation, there are grating responses with amplitudes equal to that of the main beam. At 50 MHz, these are away by  $36^\circ$  and  $59^\circ$  in the E–W and the N–S directions respectively, whereas at 150 MHz they are away by only  $11^\circ$  and  $16^\circ$ . Because of the above, there can be some confusion when interpreting those solar records which are obtained with a sidereal source present at the position of the grating lobe. It must be remembered that the above discussion is only for the one-dimensional case. When we correlate the output of each group in the E–W arm with that in the south arm, bandwidth effects may reduce the coherence of the radiation at the position of these grating lobes, as the compensating delays in the south arm are introduced for a particular declination.

The output from each of the 32 groups are amplified approximately 34 dB in a wide-band amplifier and passed through an electronic switch which periodically inverts the phase of the input signal under the control of the Walsh switching signal sent from the central receiver building. The details of the switching scheme is described in a later section. The switched RF output from each group is sent to the receiver room via open wire transmission lines because of cost considerations and also low attenuation.

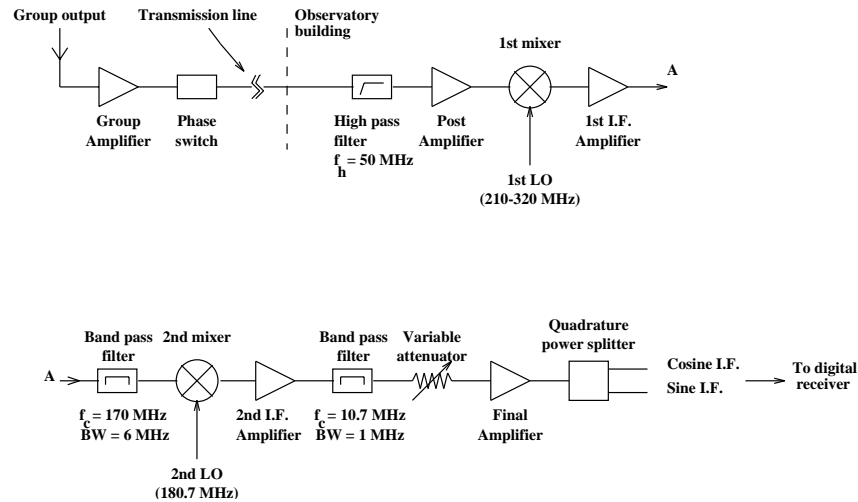


Figure 7. Schematic diagram of one of the 32 analog front-end receiver channels.

## 4. Receiver System

### 4.1. ANALOG FRONT END

In the observatory building the RF signals from the 32 antenna groups are processed separately in carefully matched amplifiers and digital networks. The RF signal from each group after getting amplified goes through two frequency conversions. It is first up-converted to an intermediate frequency (IF) of 170 MHz. This conversion places all the image frequencies well above the frequency of observation. Multi-frequency operation is achieved by switching the first local oscillator (LO) to different frequencies in the range 210 to 320 MHz. The IF signal is then passed through a bandpass filter with a center frequency ( $f_c$ ) of 170 MHz and a bandwidth (BW) of 6 MHz to suppress the spurious pick-ups through harmonics. After further amplification, the signal is down-converted to a second IF of 10.7 MHz by mixing with a fixed LO of 180.7 MHz. The output is again amplified and passed through a band pass filter with a  $f_c$  of 10.7 MHz and a BW of 1 MHz to cut-off contributions from unwanted signals at other frequencies. The IF signals from each of the 32 antenna groups are split into in-phase (cosine) and quadrature (sine) components by passing them through analog quadrature hybrids and feeding them to the digital correlator. Figure 7 shows the block diagram of the analog front-end receiver.

### 4.2. DIGITAL BACK END

In order to obtain all possible multiplications between the 32 antenna groups, a 1024-channel digital correlator is used. The layout of the digital system is shown in Figure 8. The 10.7 MHz IF signals are first quantised to two levels using a zero crossing detector. Then they are over sampled at a rate of 3.6 MHz (the required

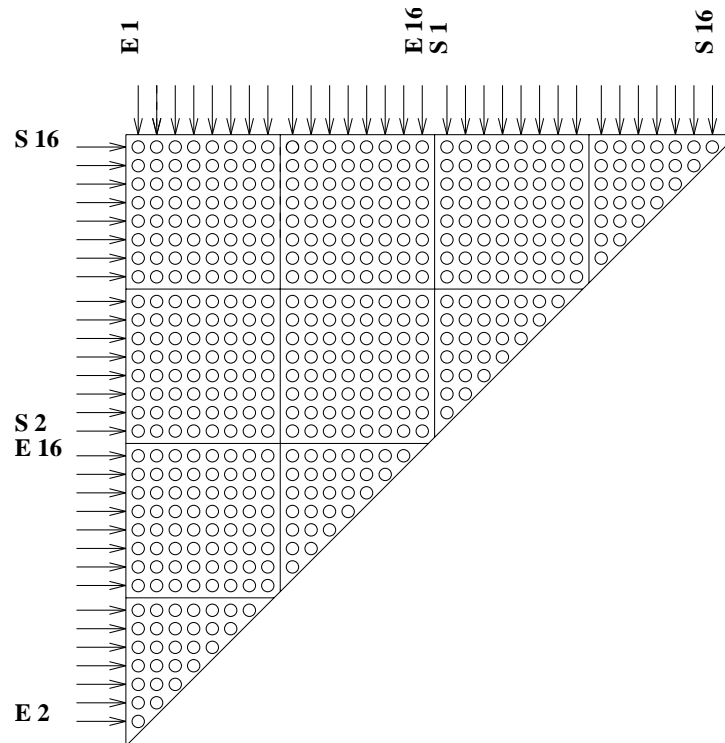


Figure 8. Lay-out of the 1024-channel digital correlator system.

Nyquist rate is 2 MHz corresponding to the 1 MHz IF bandwidth) enabling finer delay resolution which is explained below.

For observations away from the zenith with relatively large bandwidths, it is necessary to delay the signals appropriately before correlation in order to preserve coherence. The use of digital delays implies that the time delay can only be changed in discrete steps. For the 3.6 MHz sampling rate, the maximum delay error (139 ns) causes a coherence loss of about 3% for a 1 MHz bandwidth.

#### 4.3. WALSH SWITCHING

The open wire transmission lines carrying RF signal from each antenna group are well separated. The IF cables and A/D convertors are carefully shielded. In spite of these precautions it was found that there is a certain amount of crosstalk between individual signal channels which causes low level spurious correlations. We employ Walsh function phase switching to reduce this effect. Assuming that most of the crosstalk occurs between the signals flowing through the open wire lines, the RF output from each antenna group is periodically inverted using orthogonal binary sequences which control the phase switch kept in the field immediately after the group amplifier. Since the switching period is an integer fraction of the integration

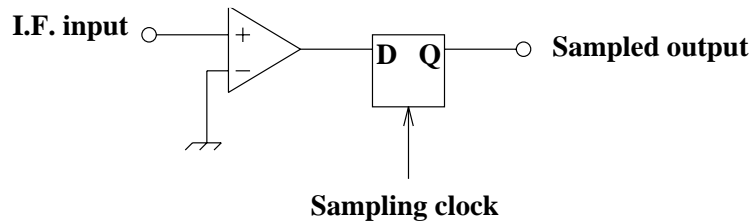


Figure 9. Block diagram of 1-bit sampler.

time, the crosstalk signals get averaged to zero as they are correlated half of the time positively and the other half negatively. This phase inversion sequence is subsequently demodulated at the output of the sampler, thereby also eliminating any errors due to possible DC offsets in the A/D converters.

#### 4.4. THE 1024-CHANNEL DIGITAL CORRELATOR

Figure 9 shows the block diagram of the 1-bit sampler. The basic element is the high-speed comparator (AD 790). The output of the comparator is a TTL signal corresponding to whether the input IF signal is below the 'ground' level or above it. This signal is then sampled in a D-type flip flop (74LS74). An Ex-OR gate (74LS86) is used to demodulate the sampled signal for Walsh switching.

After the removal of the phase inversion, the sampled signal then flows through the delay lines, which have been constructed using a combination of shift registers (74LS164) and multiplexers (74LS151). The necessary delays are implemented under the control of a computer with the maximum value of the delay being  $1.96 \mu\text{s}$ . This allows us to carry out observations of sources even at larger zenith distances without any coherence loss.

The correlator system was built using the chips designed for the Nobeyama radioheliograph, Japan. These are custom-built chips using the CMOS gate array technology. The architecture of the chip is shown in Figure 10. It accepts inputs from 4 antennas and provides 4 complex correlations corresponding to a  $(2 \times 2)$  antenna pair. Each cosine correlator gives output according to  $C_1 \oplus C_2 + S_1 \oplus S_2$  and sine correlator according to  $C_1 \oplus S_2 - C_2 \oplus S_1$ .

#### 4.5. DATA ACQUISITION

The correlator system consists of 8 boards, and 16 correlator chips are mounted on each one of them. Each board will correlate signals corresponding to  $(8 \times 8)$  antenna pairs, giving 128 correlations. At the end of each integration period (about 145 ms), correlated data from each of these 128 correlators in one board will be written into a memory unit. This operation goes on synchronously in all the 8 boards. The process of reading correlated data from each chip and writing into the memory unit goes on till we reach 256 integration cycles. During this time, i.e., when correlated data are being written into a memory unit, data which was written

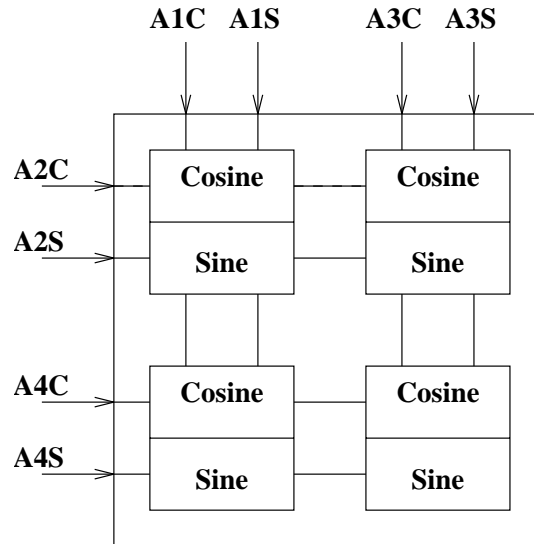


Figure 10. Functional diagram of the correlator chip.

into another memory unit during earlier 256 integration cycles will be read into a computer. At the end of 256 integration cycles, the roles of the memory units get reversed.

## 5. Calibration

The process of calibration recovers the true visibilities from the observed quantities which are often corrupted for a multitude of reasons. There are a wide variety of errors which can affect the visibility data obtained with a radio interferometer (Wieringa, 1991). Due to these errors, the observed complex visibility ( $V^{\text{obs}}$ ) on a certain baseline differs from the true response ( $V^{\text{true}}$ ), leading to inaccuracies in the determination of the source brightness distribution. Generally these errors are determined by observing calibration sources with known flux and position and which are close to the region of the sky being mapped. In practice these external methods work well for those arrays for which the pointing of the antenna beam position can be changed frequently between the calibrator and the source being observed. But in the case of low-frequency arrays like the GRH which consists of dipole antennas, changing the beam position as mentioned above is very difficult. One has to estimate the correction terms by observing a calibrator source at a different time and whose position may also be different from the field of interest. This can lead to additional problems particularly at low frequencies since the phase errors due to ionosphere can change significantly over short time scales. To alleviate these problems, we have developed a self-calibration scheme for correcting the phase errors in the observed visibilities. The errors due to gain (amplitude) variations

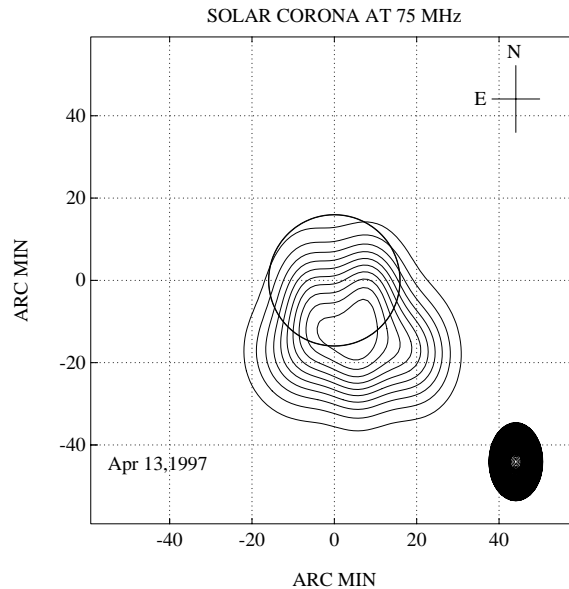


Figure 11. Noise-storm source observed with the GRH. The open circle at the center is the solar limb and the filled circle at the bottom right is the beam of the instrument.

are assumed to be less crucial since we are using one-bit correlators. The phase calibration scheme, which uses the observed field itself to estimate the error terms, is based on closure techniques and the redundancy in the length and orientation of the baseline vectors. Details of this method will be published elsewhere.

## 6. Initial Results

In the recent years, it has been pointed out by several authors that there are sources of weak noise storms on the Sun whose brightness temperatures are approximately equal to that of the quiet Sun. On the basis of two-dimensional maps obtained with the Nançay radioheliograph at 169 MHz, Alissandrakis, Lantos, and Nicolaidis (1985) have showed that these sources lie above the polarity inversion line of the underlying photospheric magnetic field. The presence of such sources have been invoked to explain the observed brightness temperature variations in the low frequency maps of the Sun (Sastry, 1994).

Figure 11 shows the radio map of the corona at 75 MHz obtained with the GRH on 13 April 1997 around 06:30 UT. One can notice the existence of a localised region close to the southwest limb which closely corresponds to the position of the polarity inversion line present in the photospheric magnetogram (*Solar Geophysical Data*, 1997) taken on the same day at 21:26 UT (Figure 12). Observations carried out with the Nançay radioheliograph at 164 MHz (Figure 13) at 09:03:30 UT indicate the presence of a strong noise-storm source at the same location. Though

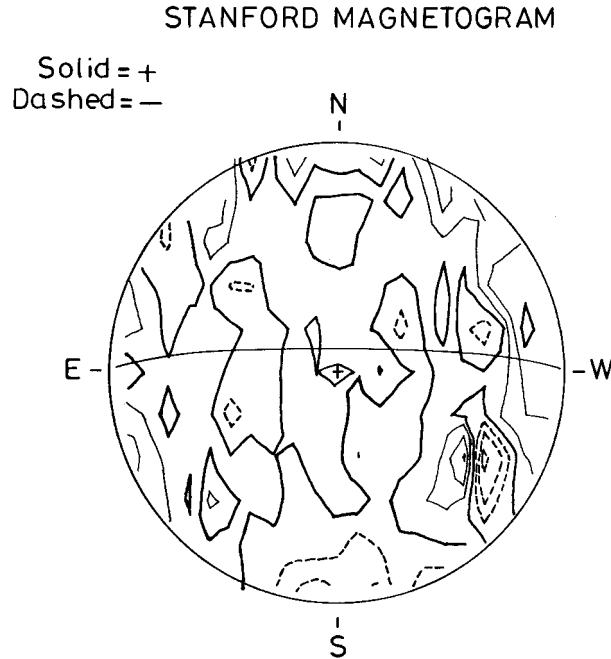


Figure 12. Photospheric magnetogram.

the source was very bright at 164 MHz, it was seen only as a weak region at 75 MHz ( $T_b \approx 0.9 \times 10^6$  K). This confirms the earlier observations by Lantos *et al.* (1987) that the noise-storm sources tend to become weaker as we move towards the lower frequencies.

Figure 14 shows a map of the solar corona obtained with the Gauribidanur radioheliograph on 23 October 1997 at 109 MHz. Figure 15 shows a similar map made with the Nançay radioheliograph at 164 MHz on the same day but about 2 hr later. There is a striking similarity between the two maps. There is an apparent shift of the peak of radio emission at 109 MHz in a northwesterly direction compared to that at 164 MHz. At the moment it is not clear whether this shift is due to refraction or the shape of the streamer/coronal condensation responsible for the emission. A detailed analysis of these maps will be published separately.

## 7. Present Status

At present, the GRH is being operated at a single frequency (changeable by tuning the first LO) as a meridian transit instrument with the observation duration limited by the primary beam of the groups in the E–W arm. Work is being carried out to install both the multi-frequency operational capability and the tracking system which will enable continuous observations of the Sun for about  $\pm 2$  hr around

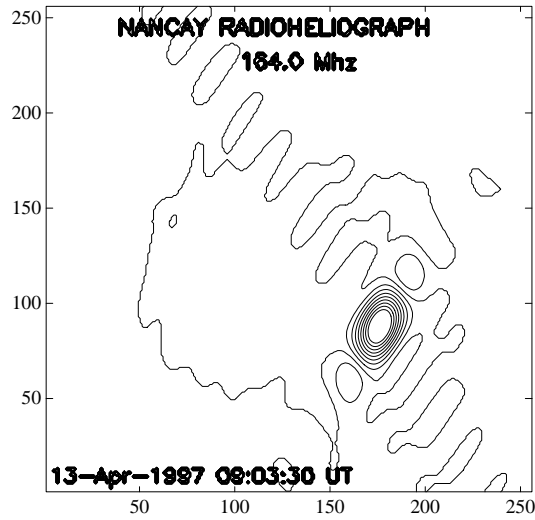


Figure 13. Observations of the same noise storm event with Nançay radioheliograph.

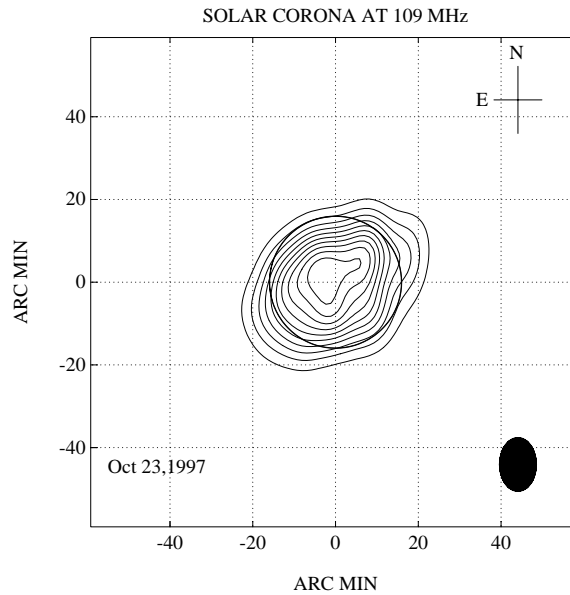


Figure 14. Map of the undisturbed Sun observed with the GRH at 109 MHz.

local noon, which is approximately 06:30 UT. The system is expected to become operational by early 1998.

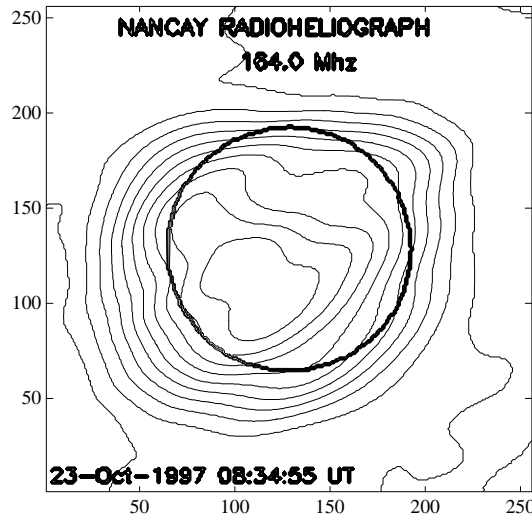


Figure 15. Same as Figure 14, but observed with the Nançay radio heliograph at 164 MHz two hours later.

## 8. Conclusion

With the Nobeyama and the Nançay radioheliographs carrying out regular observations of the Sun at centimeter and decimeter–meter wavelength ranges, respectively, it has now become possible to extend the range up to decameter wavelengths with the operation of the Gauribidanur radioheliograph. A multi-wavelength collaborative study using the data obtained with ground-based instruments and those on board space missions like *Yohkoh*, WIND, SOHO, etc., is expected to provide new insights into the Sun.

## Acknowledgements

We express our sincere thanks to Prof. R. Cowsik, Director, Indian Institute of Astrophysics, for his keen interest and kind support to the radioheliograph project. We also thank C. Nanje Gowda, A. T. Abdul Hameed, E. Ebenezer, A. Anwar Saheb, G. N. Rajasekara, and D. Babu for their help in setting of the array and the receiver system. The Nançay radioheliograph group is thanked for having allowed us to reproduce their maps. The basic design of the correlator chip was made at the Nobeyama Radio Observatory, Japan. The methods used for the amplitude and phase calibration of the heliograph evolved during our discussions with Drs Hiroshi Nakajima and Masanori Nishio, during their visit to our observatory under the Indo-Japanese collaborative program. We gratefully acknowledge their contribution to the heliograph project.

### References

- Alissandrakis, C. E., Lantos, P., and Nicolaidis, E.: 1985, *Solar Phys.* **97**, 267.  
Erickson, W. C., Mahoney, M. J., and Erb, K.: 1982, *Astrophys. J. Suppl.* **50**, 403.  
Lantos, P., Alissandrakis, C. E., Gergely, T., and Kundu, M. R.: 1987, *Solar Phys.* **112**, 325.  
Sastry, Ch. V.: 1994, *Solar Phys.* **150**, 285.  
*Solar Geophysical Data*: 1997, No. 634, part 1, p. 53.  
Wieringa, M. H.: 1991, Ph.D. Thesis, University of Leiden.